Anisotropic Mesh Adaptation for Large Eddy Simulations

Robin Barbera, Thomas Berthelon, Roxane Letournel, Giovanni Ghigliotti, Guillaume Balarac

Anisotropic mesh adaptation for Large Eddy Simulations

R. Barbera*
Université Grenoble Alpes, CNRS, Grenoble-INP, LEGI, 38000 Grenoble, France
Safran Tech, Modelling and Simulation, 78772 Magny-les-Hameaux, France

T. Berthelon†
Université Grenoble Alpes, CNRS, Grenoble-INP, LEGI, 38000 Grenoble, France

R. Letournel‡
Safran Tech, Modelling and Simulation, 78772 Magny-les-Hameaux, France

G. Ghigliotti§ and G. Balarac¶
Université Grenoble Alpes, CNRS, Grenoble-INP, LEGI, 38000 Grenoble, France

This paper aims at developing an anisotropic mesh adaptation strategy for Large Eddy Simulation (LES) of industrial applications. Starting from the Isotropic Automatic Mesh Convergence (IAMC) strategy developed in [1] and extended in [2] and using the anisotropic remeshing methodologies initially developed for RANS, we propose a novel Anisotropic Automatic Mesh Convergence (AAMC) strategy to ensure similar LES accuracy, but with fewer mesh elements than with the IAMC strategy. As with the IAMC strategy, this new strategy is designed to ensure proper mean flow resolution and that enough turbulent scales are resolved in fully turbulent regions to perform reliable LES. However, particular attention is needed to ensure that the primary instabilities leading to the transition to turbulence are correctly accounted for with the anisotropic meshes.

I. Introduction

In recent years, following the CFD Vision 2030 report [3], the development of the methodology along with the increase in available computing power has encouraged the use of Large Eddy Simulation (LES) for industrial cases [2, 4–8]. A key component of these applications is the mesh adaptation procedure, as it allows to concentrate the computational effort on regions of interest [9–13].

Nowadays, in LES, these methods are mainly applied with isotropic meshes, but anisotropic meshes could be an important ingredient to reduce the computational cost, allowing to reduce both the number of elements and the computational time, as well as the time to solution. The framework for anisotropic mesh adaptation was developed in the early 2000s [14] first for two-dimensional calculations [15, 16] and then quickly for three-dimensional calculations [17]. Today, it allows for accurate control of numerical error [18, 19] in various norms [20] and these methods are widely used for RANS applications [21] both in aerospace [22–24] and turbomachinery [25, 26] with significant reduction in computational complexity.

The aim of this work is to extend the use of anisotropic meshes to LES in order to achieve high fidelity simulation at a lower cost. Furthermore, as the meshing process in today's CFD is a complex and time-consuming task, we aim at proposing an automatic numerical framework to build anisotropic meshes with accurate numerical error control. This methodology should automatically capture all the physical features of the flow starting from an initial coarse grid. For this purpose, the statistical mesh adaptation strategy proposed in [1] and [2] originally used in an isotropic framework will be adapted to an anisotropic framework. Particular attention will be paid to correctly capture coherent structures to maintain LES accuracy.

In this paper, the current isotropic framework for static mesh refinement of LES is first presented and applied to the LES of a turbulent round jet flow configuration. The adapted mesh definition is based on two criteria: the first is a

*PhD Student, robin.barbera@univ-grenoble-alpes.fr
†Research Engineer, thomas.berthelon@univ-grenoble-alpes.fr
‡Research Engineer, roxane.letournel@safrangroup.com.
§Associate professor, giovanni.ghigliotti@univ-grenoble-alpes.fr
¶Professor, guillaume.balarac@univ-grenoble-alpes.fr

feature-based error estimator and the second ensures the resolution of sufficient turbulent scales in a LES context. The extension of this methodology to an anisotropic framework is then proposed and limitations are shown for the region with transition to the turbulence. In order to address these issues, the last part of this work focuses on the development of a new criterion for the detection and remeshing of these transition regions.

II. LES strategies for isotropic meshes

This work has been carried out using the YALES2 flow solver [27]. It solves the incompressible Navier-Stokes equations on unstructured meshes based on a projection method for pressure-velocity coupling [28] using a highly efficient linear solvers [29]. Explicit time integration was used for the convective terms with a modified fourth-order Runge-Kutta scheme [30] and semi-implicit integration for the diffusive terms. The use of unstructured meshes along with the double decomposition domain in the YALES2 library allows LES and DNS of complex geometries to be performed in the context of massively parallel computation. Parts of the mesh adaptation process are based on the isotropic and anisotropic mesh adaptation library MMG [31] in a parallel mesh adaptation strategy described in [32]. The solver has been validated for various applications including combustion [33, 34], biomechanics [35], hydroelectricity [36] or wind energy [37].

The Isotropic Automatic Mesh Convergence (IAMC) framework introduced in [1] is based on the alternance of statistics accumulation phases followed by isotropic mesh adaptations. Its aim is to ensure the accuracy of the LES by guaranteeing an adequate mesh. This strategy results in an automatic, robust and user-independent procedure, and it has been extensively used for various applications [1, 2, 4, 5] applications. The objective of the IAMC procedure is to obtain mesh independence of the energy balance of the mean field, by ensuring mesh independence of the molecular dissipation and turbulent production terms [2]. This is achieved through the use of two criteria, the first one based on the control of the interpolation error of the mean field, and the second one ensuring the resolution of sufficient turbulent scales for LES.

Based on previous works [14, 18, 38], it can be shown that the error on the mean field on an isotropic mesh with a cell size h can be bounded by

$$QC_1 = h^2 \mathcal{H}_f, \tag{1}$$

where $\mathcal{H}_f$ is the highest absolute eigenvalue of the Hessian of the time-averaged quantity of interest f (here the kinetic energy of the mean field). This leads to the determination of the isotropic adapted cell size, h_{QC_1},

$$h_{QC_1} = \sqrt{\frac{QC_{1,T}}{\mathcal{H}_f}}, \tag{2}$$

where $QC_{1,T}$ is the constant target value for the error on the quantity of interest to control and make uniform the error in the overall computational domain.

However, an additional constraint has to be applied to the mesh size (acting as the filter size) to explicitly resolve enough turbulent scales and then ensure reliable LES. It can be shown that for fully turbulent flows at least 80% of the turbulent kinetic energy (TKE) must be explicitely resolved [39]. Therefore, a second criterion based on the TKE resolution is used. By defining the explicitly resolved TKE, $K^>$, and the unresolved (modeled) TKE, $K^<$, the second criterion is thus defined as this ratio [1, 2],

$$Qc_2 = \frac{K^<}{K^> + K^<}. \tag{3}$$

Based on the theoretical behavior of the subgrid-scale (SGS) model with the decrease of the mesh size [39, 40], an estimation of the isotropic adapted cell size due to this criterion is

$$h_{QC_2} = h\Big(\frac{QC_{2,T}}{QC_2}\Big)^{3/2}, \tag{4}$$

with $QC_{2,T}$ the targeted quantity of unresolved kinetic energy set to 0.2 and h the cell size of the current mesh. The final isotropic adapted cell size is then defined as the minimum value between h_{QC_1} and h_{QC_2}.

Application of the methodology to the turbulent round jet flow

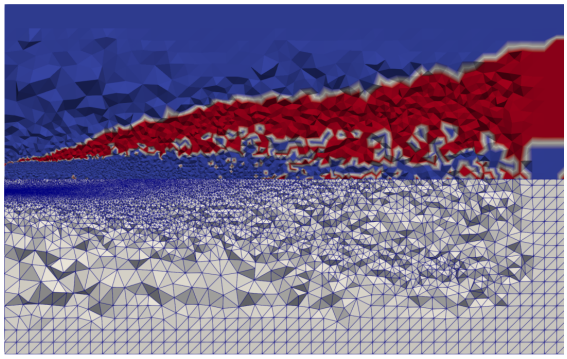

(a) Illustration of the adapted mesh at the center plane of the jet (bottom) and center plane colored by a map showing where QC_1 (in blue) and QC_2 (in red) control the local cell size (top).

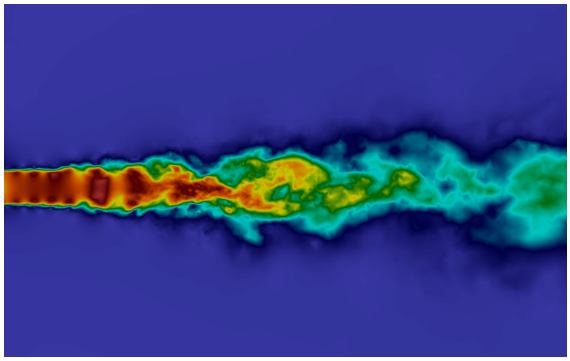

(b) Center plane coloured by the non-dimensional instantaneous velocity norm

Fig. 1 IAMC strategy applied to the turbulent round jet

As in [2], the presented methodology is now applied to a canonical turbulent round jet in co-flow with a Reynolds number $Re = 4000$. The only notable difference is the use of the σ subgrid-scale model [41] instead of the dynamic Smagorinsky model [42]. Starting from an initial coarse mesh (with uniform cell size equal to one inlet radius of the jet) the IAMC procedure converges to the adapted mesh shown in Fig. 1a. As expected, close to the jet inlet, the cell sizes are smaller in the shear layer where the highest mean velocity gradients are found (Fig. 1b). In this region the cell size is then controled by the QC_1 criterion (Fig. 1a). This leads to the development of Kelvin-Helmholtz instabilities, and then to the transition of the flow to a turbulent state. This transition results in an increase in small-scale turbulence and a reduction in mean velocity gradients due to turbulent diffusion. In the turbulent region, the cell size is predominantly controlled by the QC_2 criterion.

III. Extension to anisotropic meshes

This strategy is now extended to anisotropic meshes to be able to propose a Anisotropic Automatic Mesh Convergence (AAMC). For anisotropic mesh adaptation, the metric is a tensor field (whereas in the isotropic case it is a scalar characterizing the cell size), which allows to take into account different sizes in different directions. This tensor field is used to define the local cell size and orientation throughout the domain. The use of such an anisotropic metric tensor is widely studied in the literature [14, 15, 20] and only a short introduction will be given in this article (see [20, 43] for details).

The metric tensor $\mathcal{M}$ is symmetric and positive-definite, so it can be decomposed into

$$\mathcal{M} = \mathcal{R}\begin{pmatrix}\lambda_1 & 0 & 0\\ 0 & \lambda_2 & 0\\ 0 & 0 & \lambda_3\end{pmatrix}\mathcal{R}^T = \mathcal{R}\Lambda\mathcal{R}^T, \tag{5}$$

with $\mathcal{R}$ the orthonormal matrix composed of the eigenvectors $\mathbf{v_i}$ of $\mathcal{M}$,

$$\mathcal{R} = (\mathbf{v_1}\ \ \mathbf{v_2}\ \ \mathbf{v_3})$$

which are two-by-two orthogonal, and Λ is a diagonal matrix composed of the eigenvalues λ_i of $\mathcal{M}$. These eigenvalues characterize the cell size specification h_i in this basis, $\lambda_i = \frac{1}{h_i^2}$.

In this context, the first mesh adaptation criteria proposed to control the error on the mean field discretization [14]

can be written as,

$$\mathcal{M}_{QC_1} = \frac{1}{QC_{1,T}}|\mathcal{H}| = \mathcal{R}\begin{pmatrix} \frac{|\lambda_1|}{QC_1} & 0 & 0 \\ 0 & \frac{|\lambda_2|}{QC_1} & 0 \\ 0 & 0 & \frac{|\lambda_3|}{QC_1} \end{pmatrix}\mathcal{R}^T, \tag{6}$$

with $QC_{1,T}$ the desired maximum interpolation error and $\mathcal{H}$ the Hessian of the discretized quantity of interest (here the kinetic energy of the mean field). Note that the isotropic formula Eq. 1 is just a particular case of this formulation where the smallest cell size is taken.

Since the QC_2 criterion (Eq. 3) is used to define the filter size of the LES approach, it is expected to stay isotropic. This criterion remains unchanged for anisotropic meshes, leading to a diagonal metric tensor,

$$\mathcal{M}_{QC_2} = \begin{pmatrix} h_{QC_2}^{-2} & 0 & 0 \\ 0 & h_{QC_2}^{-2} & 0 \\ 0 & 0 & h_{QC_2}^{-2}. \end{pmatrix} \tag{7}$$

Both metric tensors are then intersected [44, 45] to keep only the most restrictive criterion in each direction and to ensure a mesh that satisfies both criteria throughout the domain. An anisotropic cell size gradation [46, 47] and maximum anisotropy are also imposed on the metric field before the remeshing process to ensure a regular enough mesh in adequation with the numerical methods used.

Application of the methodology to the turbulent round jet flow

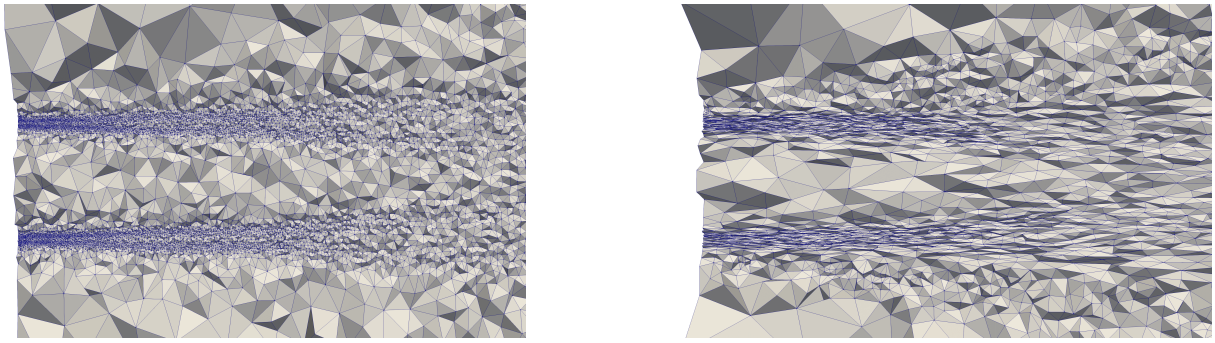

(a) Isotropic mesh **(b) Anisotropic mesh**

Fig. 2 Isotropic and anisotropic mesh comparison in the near-field region of the jet

The presented methodology has been applied to the turbulent round jet in co-flow test case in order to compare the isotropic and anisotropic mesh adaptation strategies. The resulting anisotropic mesh shows highly anisotropic cells in the shear layer in the near-field of the jet, resulting in a total number of elements divided by 4 compared to the isotropic case (Fig. 2b). Indeed, as shown in the previous section, the mesh adaptation in this region is controlled by the rapid variation of the mean field in the radial direction. Downstream, when the turbulence is more developed, the QC_2 criterion takes over, leading to identical mesh for the isotropic and anisotropic simulations (not shown). However these anisotropic cells (up to an aspect ratio of 60) in the near-field, do not allow to correctly describe the development of the Kelvin-Helmholtz instability in this region, as seen in Fig. 3 where the instantaneous vorticity field is strongly distorted and smoothed by the anisotropic cells, in comparison with the isotropic case.

This incorrect representation of the primary jet instability has consequences on the statistical quantities. Fig. 4 represent the mean and the rms (root-mean-squared) velocity profiles close the jet inlet (at a distance $x/D = 1$ where D is the jet diameter). The mean field is well discretized on the anisotropic mesh, but the fluctuating part is strongly underestimated. This emphasizes the fact that another criterion must be used in the context of anisotropic mesh refinement of turbulent flows, in order to accurately describe the flow in regions where transition to turbulence occurs.

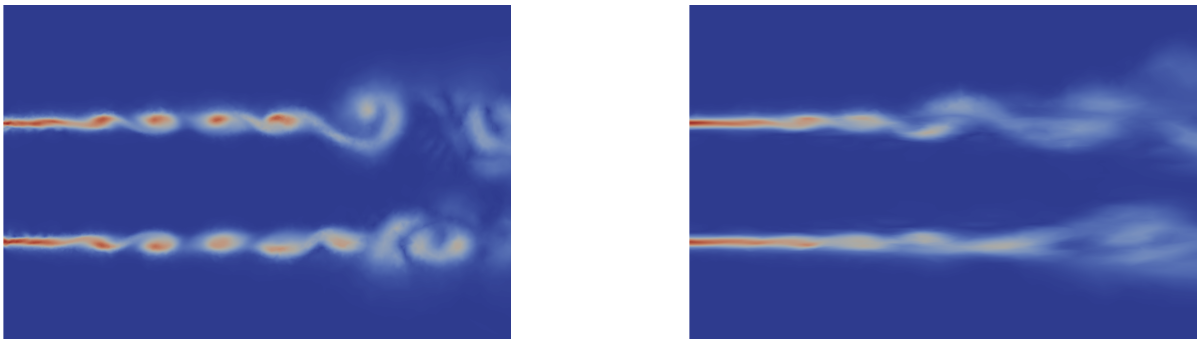

(a) Isotropic mesh **(b) Anisotropic mesh**

Fig. 3 Instantaneous vorticity norm in the near-field of the jet.

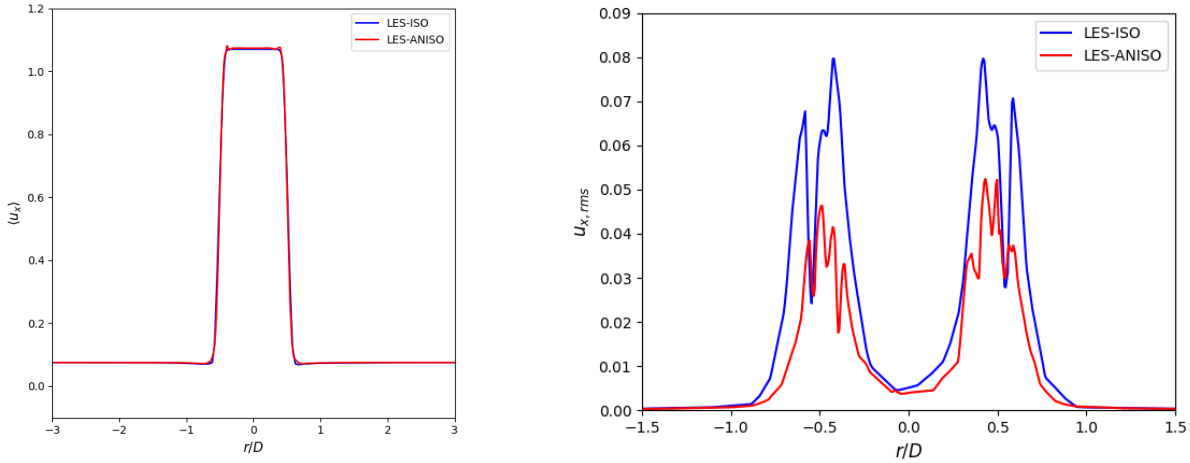

(a) Mean axial velocity **(b) rms axial velocity**

Fig. 4 Mean and rms axial velocity profile at $x/D = 1$

Note that these regions cannot be described using the QC_2 criterion (guaranteeing the resolution of enough turbulent scale), because there are no (or few) modeled turbulent scales (the SGS model is expected to vanish in this region). On the other hand, these regions show transient phenomena (Kelvin-Helmholtz instability in the round jet case) that are not captured by the mean flow criterion (QC_1), which therefore leads to highly anisotropic cells.

IV. Preliminary results: towards a new criterion for the anisotropic remeshing of transition regions in the turbulence

The previous section highlights the fact that the current isotropic mesh adaptation methodology, which is based on the accurate mean field discretization and the resolution of enough turbulent scales, lacks a criterion for the region of development of turbulence. These regions exhibit transient features that need to be resolved, but are not fully developed in terms of turbulence. This section of preliminary results aims to fill this gap by proposing a new criterion in order to develop a robust strategy for the static anisotropic remeshing of LES. The first part of this section is devoted to the presentation of such a criterion, which will later be used to detect the transition region on the round jet flow, where a dedicated time-accurate metric needs to be applied.

The physical detection of turbulent features of a flow is a topic already assessed in the construction of a subgrid-scale model for LES. The σ-model [41] takes advantage of the singular values of the velocity gradient tensor to vanish when the flow exhibits two-dimensional or two-component features, or in the case of pure shear, which are flow characteristics

expected in transition regions. Starting from the velocity gradient tensor $\mathbf{g}$ (with $g_{ij} = \partial u_i/\partial x_j$), its singular values $\sigma_1 \geq \sigma_2 \geq \sigma_3$ are the square roots of the eigenvalues of $\mathbf{G} = \mathbf{g}^T\mathbf{g}$. The smallest singular value σ_3 is null when a row or a column of $\mathbf{g}$ is zero, which implies that the flow is two-dimensional. Furthermore, pure axisymmetric expansion or contraction are detected when $\sigma_2 = \sigma_3$ or $\sigma_1 = \sigma_2$. The eddy-viscosity of the σ-model is then constructed as follows,

$$\nu_{SGS} = (C_\sigma h)^2 \frac{\sigma_3(\sigma_1 - \sigma_2)(\sigma_2 - \sigma_3)}{\sigma_1^2} \tag{8}$$

with h the local (isotropic) cell size and C_σ a constant, to guarantee that the eddy-viscosity vanishes in two-dimensional flow regions or in pure shear flow regions.

In this work, a sensor to identify these regions is adapted from this model,

$$\sigma_{sensor} = \frac{\sigma_3(\sigma_1 - \sigma_2)(\sigma_2 - \sigma_3)}{\sigma_1^3}. \tag{9}$$

Small enough value of σ_{sensor} allows then to identify transition regions where a specific adapted metric needs to be computed. In the detected regions, the metric is constructed by performing a time intersection of the metrics computed on the instantaneous resolved kinetic energy, as introduced in [48] and [49].

Application to the jet flow test case

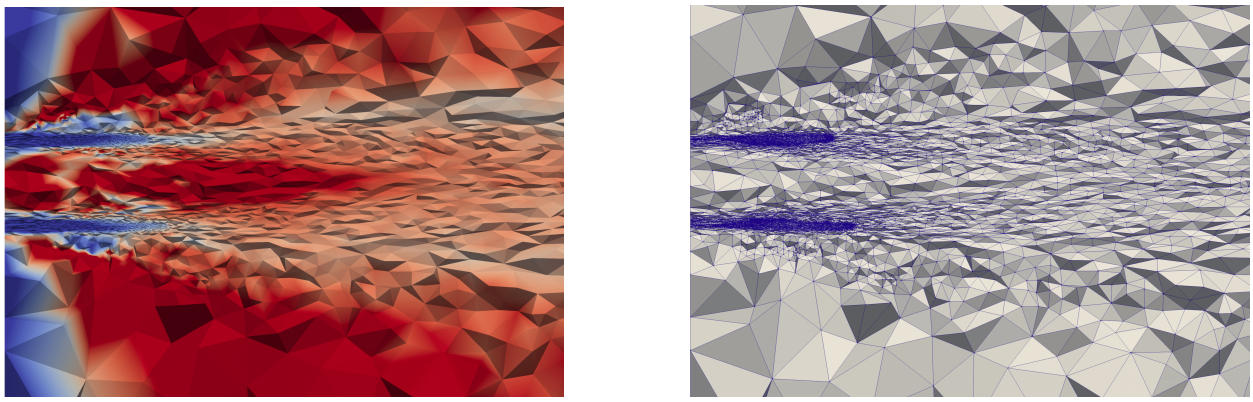

(a) σ_{sensor} field (null values in blue) **(b) Close up view on the mesh around the σ_{sensor}**

Fig. 5 Anisotropic mesh using the σ_{sensor}

This new strategy is now applied to the LES of the turbulent round jet. As expected, σ_{sensor} has high values when the turbulence is developed, and tends to vanish when the flow exhibits transient characteristics. This is shown in Fig. 5a where σ_{sensor} tends to 0 (blue) in the shear layers in the near-field of the jet, which is indeed the region that requires a small enough mesh size to properly trigger the Kelvin-Helmholtz instability. The transition region is detected using a threshold on this sensor. In the detected regions, the adapted metric based on the instantaneous resolved kinetic energy leads to a strong refinement and a reduction of the cell anisotropy (Fig. 5b).

This strategy accurately describes the transient behavior in the near-field of the jet and accurately triggers the Kelvin-Helmholtz instabilities. This then allows the estimation of the rms axial velocity to be corrected (Fig. 6). However, it should be emphasized that the increased number of elements in the σ_{sensor} region only leads to a 35% reduction in the number of elements compared to the classical isotropic case (while the anisotropic mesh described in Sec. III leads to a 75% reduction).

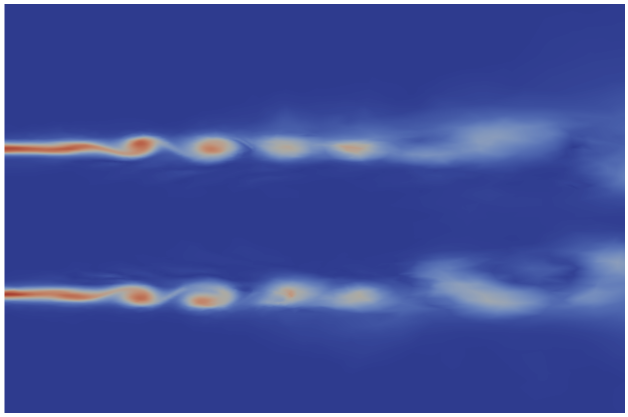

(a) Instantaneous vorticity norm in the near-field of the jet

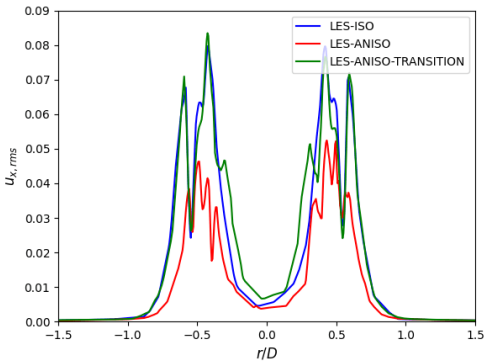

(b) rms axial velocity profile at $x/D = 1$

Fig. 6 Results for the anisotropic mesh with the transition criterion

V. Conclusions and perspectives

In this work, the YALES2 automatic mesh convergence procedure for isotropic meshes for LES developed in [1] and [2] is adapted to anisotropic mesh framework. A limitation of this strategy is pointed out, consisting in inaccurate resolution of the regions where the transition to turbulence occurs. An original methodology based on a turbulence sensor is proposed to solve this problem. The test case shows a significant improvement in terms of accuracy in the region of transition to turbulence, with an accuracy close to the isotropic mesh case.

Next perspectives for this work are to optimize the strategies around the σ sensor and metric construction in this region and to apply the presented methodology to other academic and pre-industrial cases.

Acknowledgments

This work was granted access to the HPC resources of CINES/TGCC/IDRIS under the projects 22A00611 made by GENCI. Part of this work has been initiated during the Extreme CFD Workshop & Hackathon (https://ecfd.coria-cfd.fr). TB and GB gratefully acknowledge support from NETHUNS project under grant ANR-21-CHIN- 0001-01.

References

[1] Benard, P., Balarac, G., Moureau, V., Dobrzynski, C., Lartigue, G., and D'Angelo, Y., "Mesh adaptation for large-eddy simulations in complex geometries," *International Journal for Numerical Methods in Fluids*, Vol. 81, No. 12, 2016, pp. 719–740. https://doi.org/https://doi.org/10.1002/fld.4204, URL https://onlinelibrary.wiley.com/doi/abs/10.1002/fld.4204.

[2] Grenouilloux, A., Leparoux, J., Moureau, V., Balarac, G., Berthelon, T., Mercier, R., Bernard, M., Bénard, P., Lartigue, G., and Métais, O., "Toward the use of LES for industrial complex geometries. Part I: automatic mesh definition," *Journal of Turbulence*, Vol. 24, No. 6-7, 2023, pp. 280–310.

[3] Slotnick, J. P., Khodadoust, A., Alonso, J., Darmofal, D., Gropp, W., Lurie, E., and Mavriplis, D. J., "CFD vision 2030 study: a path to revolutionary computational aerosciences," Tech. rep., 2014.

[4] Alloin, E., Balarac, G., Métais, O., Laurant, L., and Ségoufin, C., "Large Eddy Simulations of the part-load instability in a Pump-Turbine in pump mode," *25e Congrès Français de Mécanique, Nantes, 29 août-2 septembre 2022*, 2022.

[5] Puggelli, S., Leparoux, J., Brunet, C., Mercier, R., Liberatori, L., Zurbach, S., Cabot, G., and Grisch, F., "Application of an automatic mesh convergence procedure for the large eddy simulation of a multipoint injection system," *Journal of Engineering for Gas Turbines and Power*, Vol. 145, No. 6, 2023, p. 061019.

[6] Bauerheim, M., "Theoretical and numerical study of symmetry breaking effects on azimuthal thermoacoustic modes in annular combustors," Ph.D. thesis, Institut National Polytechnique de Toulouse-INPT, 2014.

[7] Lehmkuhl, O., Park, G., Bose, S., and Moin, P., "Large-eddy simulation of practical aeronautical flows at stall conditions," *Proceedings of the 2018 Summer Program, Center for Turbulence Research, Stanford University*, Vol. 87, 2018.

[8] Guillaud, N., Balarac, G., and Goncalvès, E., "Large eddy simulations on a pitching airfoil: Analysis of the reduced frequency influence," *Computers & Fluids*, Vol. 161, 2018, pp. 1–13.

[9] Benard, P., "Analyse et amélioration d'une chambre de combustion centimétrique par simulations aux grandes échelles," Ph.D. thesis, Rouen, INSA, 2015.

[10] Park, M. A., Kleb, W. L., Anderson, W. K., Wood, S. L., Balan, A., Zhou, B. Y., and Gauger, N. R., "Exploring Unstructured Mesh Adaptation for Hybrid Reynolds-Averaged Navier–Stokes/Large Eddy Simulation," *AIAA Scitech 2020 Forum*, 2020, p. 1139.

[11] Daviller, G., Brebion, M., Xavier, P., Staffelbach, G., Müller, J.-D., and Poinsot, T., "A mesh adaptation strategy to predict pressure losses in les of swirled flows," *Flow, Turbulence and Combustion*, Vol. 99, 2017, pp. 93–118.

[12] Agostinelli, P., Rochette, B., Laera, D., Dombard, J., Cuenot, B., and Gicquel, L., "Static mesh adaptation for reliable large eddy simulation of turbulent reacting flows," *Physics of Fluids*, Vol. 33, No. 3, 2021.

[13] Pertant, S., "Simulation numérique d'écoulements diphasiques avec ligne triple et changement de phase sur maillages non structurés," Ph.D. thesis, Université Grenoble Alpes [2020-....], 2022.

[14] Habashi, W. G., Dompierre, J., Bourgault, Y., Ait-Ali-Yahia, D., Fortin, M., and Vallet, M.-G., "Anisotropic mesh adaptation: Towards user-independent, mesh-independent and solver-independent CFD. Part I: General principles," *International Journal for Numerical Methods in Fluids*, Vol. 32, No. 6, 2000, pp. 725–744.

[15] Dompierre, J., Vallet, M.-G., Bourgault, Y., Fortin, M., and Habashi, W. G., "Anisotropic mesh adaptation: towards user-independent, mesh-independent and solver-independent CFD. Part III. Unstructured meshes," *International journal for numerical methods in fluids*, Vol. 39, No. 8, 2002, pp. 675–702.

[16] Venditti, D. A., and Darmofal, D. L., "Anisotropic grid adaptation for functional outputs: application to two-dimensional viscous flows," *Journal of Computational Physics*, Vol. 187, No. 1, 2003, pp. 22–46.

[17] Frey, P.-J., and Alauzet, F., "Anisotropic mesh adaptation for CFD computations," *Computer methods in applied mechanics and engineering*, Vol. 194, No. 48-49, 2005, pp. 5068–5082.

[18] Loseille, A., and Alauzet, F., "Continuous mesh framework part I: well-posed continuous interpolation error," *SIAM Journal on Numerical Analysis*, Vol. 49, No. 1, 2011, pp. 38–60.

[19] Loseille, A., and Alauzet, F., "Continuous mesh framework part II: validations and applications," *SIAM Journal on Numerical Analysis*, Vol. 49, No. 1, 2011, pp. 61–86.

[20] Alauzet, F., and Loseille, A., "A decade of progress on anisotropic mesh adaptation for computational fluid dynamics," *Computer-Aided Design*, Vol. 72, 2016, pp. 13–39.

[21] Alauzet, F., and Frazza, L., "Feature-based and goal-oriented anisotropic mesh adaptation for RANS applications in aeronautics and aerospace," *Journal of Computational Physics*, Vol. 439, 2021, p. 110340.

[22] Mavriplis, J., "Results from the 3rd drag prediction workshop using the NSU3D unstructured mesh solver. AIAA Paper 2007-0256," *45th AIAA Aerospace Sciences Meeting and Exhibit, Reno, NV*, 2007.

[23] Rumsey, C. L., and Slotnick, J. P., "Overview and summary of the second AIAA high-lift prediction workshop," *Journal of Aircraft*, Vol. 52, No. 4, 2015, pp. 1006–1025.

[24] Rumsey, C., Long, M., Stuever, R., et al., "Summary of the first AIAA CFD high lift prediction workshop: AIAA 2011-0939," Tech. rep., Reston: AIAA, 2011.

[25] Charbonnier, D., Ott, P., Jonsson, M., Ko¨ bke, T., and Cottier, F., "Comparison of numerical investigations with measured heat transfer performance of a film cooled turbine vane," *Turbo Expo: Power for Land, Sea, and Air*, Vol. 43147, 2008, pp. 571–582.

[26] Casartelli, E., Mangani, L., Roos Launchbury, D., and Del Rio, A., "Application of advanced RANS turbulence models for the prediction of turbomachinery flows," *Journal of Turbomachinery*, Vol. 144, No. 1, 2022, p. 011008.

[27] Moureau, V., Domingo, P., and Vervisch, L., "Design of a massively parallel CFD code for complex geometries," *Comptes rendus. Mécanique*, Vol. 339, No. 2-3, 2011, pp. 141–148.

[28] Chorin, A. J., "Numerical solution of the Navier-Stokes equations," *Mathematics of computation*, Vol. 22, No. 104, 1968, pp. 745–762.

[29] Malandain, M., Maheu, N., and Moureau, V., "Optimization of the deflated conjugate gradient algorithm for the solving of elliptic equations on massively parallel machines," *Journal of Computational Physics*, Vol. 238, 2013, pp. 32–47.

[30] Kraushaar, M., "Application of the compressible and low-Mach number approaches to Large-Eddy Simulation of turbulent flows in aero-engines," Ph.D. thesis, 2011.

[31] Dobrzynski, C., and Frey, P., "Anisotropic Delaunay Mesh Adaptation for Unsteady Simulations," *Proceedings of the 17th International Meshing Roundtable*, edited by R. V. Garimella, Springer Berlin Heidelberg, Berlin, Heidelberg, 2008, pp. 177–194.

[32] Balarac, G., Basile, F., Bénard, P., Bordeu, F., Chapelier, J.-B., Cirrottola, L., Caumon, G., Dapogny, C., Frey, P., Froehly, A., et al., "Tetrahedral remeshing in the context of large-scale numerical simulation and high performance computing," *MathematicS In Action*, Vol. 11, No. 1, 2022, pp. 129–164.

[33] Moureau, V., Domingo, P., and Vervisch, L., "From large-eddy simulation to direct numerical simulation of a lean premixed swirl flame: Filtered laminar flame-pdf modeling," *Combustion and Flame*, Vol. 158, No. 7, 2011, pp. 1340–1357.

[34] Guedot, L., Lartigue, G., and Moureau, V., "Design of implicit high-order filters on unstructured grids for the identification of large-scale features in large-eddy simulation and application to a swirl burner," *Physics of Fluids*, Vol. 27, No. 4, 2015.

[35] Chnafa, C., Mendez, S., and Nicoud, F., "Image-based large-eddy simulation in a realistic left heart," *Computers & Fluids*, Vol. 94, 2014, pp. 173–187.

[36] Wilhelm, S., Balarac, G., Métais, O., and Ségoufin, C., "Analysis of head losses in a turbine draft tube by means of 3D unsteady simulations," *Flow, Turbulence and Combustion*, Vol. 97, 2016, pp. 1255–1280.

[37] Bénard, P., Viré, A., Moureau, V., Lartigue, G., Beaudet, L., Deglaire, P., and Bricteux, L., "Large-Eddy Simulation of wind turbines wakes including geometrical effects," *Computers and Fluids*, Vol. 173, 2018, pp. 133–139. https://doi.org/10.1016/j.compfluid.2018.03.015, URL https://hal.science/hal-02107334.

[38] Céa, J., "Approximation variationnelle des problèmes aux limites," *Annales de l'institut Fourier*, Vol. 14, 1964, pp. 345–444.

[39] Pope, S. B., "Turbulent Flows," Vol. 12, No. 11, 2001, p. 2020. https://doi.org/10.1088/0957-0233/12/11/705, URL https://dx.doi.org/10.1088/0957-0233/12/11/705.

[40] *Introduction to Turbulence in Fluid Mechanics*, Springer Netherlands, Dordrecht, 2008, pp. 1–23. https://doi.org/10.1007/978-1-4020-6435-7_1, URL https://doi.org/10.1007/978-1-4020-6435-7_1.

[41] Nicoud, F., Toda, H. B., Cabrit, O., Bose, S., and Lee, J., "Using singular values to build a subgrid-scale model for large eddy simulations," *Physics of fluids*, Vol. 23, No. 8, 2011.

[42] Germano, M., Piomelli, U., Moin, P., and Cabot, W. H., "A dynamic subgrid-scale eddy viscosity model," *Physics of Fluids A: Fluid Dynamics*, Vol. 3, No. 7, 1991, pp. 1760–1765. https://doi.org/10.1063/1.857955, URL https://doi.org/10.1063/1.857955.

[43] Balan, A., Park, M. A., Wood, S. L., Anderson, W. K., Rangarajan, A., Sanjaya, D. P., and May, G., "A review and comparison of error estimators for anisotropic mesh adaptation for flow simulations," *Computers Fluids*, Vol. 234, 2022, p. 105259. https://doi.org/https://doi.org/10.1016/j.compfluid.2021.105259, URL https://www.sciencedirect.com/science/article/pii/S0045793021003601.

[44] McKenzie, S., Dompierre, J., Turcotte, A., and Meng, E., "On metric tensor representation, intersection, and union," *11th ISGG conference on numerical grid generation*, 2009.

[45] Barral, N., "Time-accurate anisotropic mesh adaptation for three-dimensional moving mesh problems," Ph.D. thesis, Université Pierre et Marie Curie-Paris VI, 2015.

[46] Alauzet, F., "Size gradation control of anisotropic meshes," *Finite Elements in Analysis and Design*, Vol. 46, No. 1-2, 2010, pp. 181–202.

[47] Tenkes, L.-M., and Alauzet, F., "Size gradation control for anisotropic hybrid meshes," *Numerical Geometry, Grid Generation and Scientific Computing: Proceedings of the 10th International Conference, NUMGRID 2020/Delaunay 130, Celebrating the 130th Anniversary of Boris Delaunay, Moscow, Russia, November 2020*, Springer, 2021, pp. 127–139.

[48] Alauzet, F., Frey, P. J., George, P.-L., and Mohammadi, B., "3D transient fixed point mesh adaptation for time-dependent problems: Application to CFD simulations," *Journal of Computational Physics*, Vol. 222, No. 2, 2007, pp. 592–623.

[49] Alauzet, F., Loseille, A., and Olivier, G., "Time-accurate multi-scale anisotropic mesh adaptation for unsteady flows in CFD," *Journal of Computational Physics*, Vol. 373, 2018, pp. 28–63.